Quantum Spin Hall Effect and Tunable Spin Transport in As-Graphane

L. Z. Zhang,[†,‡] F. Zhai,[§] Kyung-Hwan Jin,[‡] B. Cui,[‡] Bing Huang,[∥,‡] Zhiming Wang,[*,†] J. Q. Lu,[§] and Feng Liu[*,‡,⊥]

[†]Institute of Fundamental and Frontier Sciences, University of Electronic Science and Technology of China, Chengdu 610054, China

[‡]Department of Materials Science and Engineering, University of Utah, Salt Lake City, Utah 84112, United States

[§]Department of Physics and Institute for Functional Nanomaterials, Univeristy of Puerto Rico, Mayaguez, Puerto Rico 00681, United States

[∥]Beijing Computational Science Research Center, Beijing 100193, China

[⊥]Collaborative Innovation Center of Quantum Matter, Beijing 100084, China

S Supporting Information
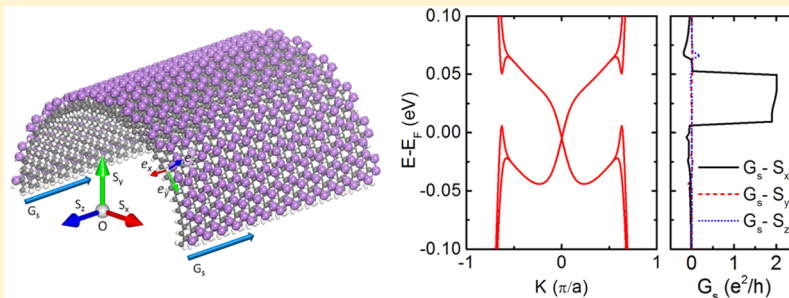
ABSTRACT: Tunable spin transport in nanodevices is highly desirable to spintronics. Here, we predict existence of quantum spin Hall effects and tunable spin transport in As-graphane, based on first-principle density functional theory and tight binding calculations. Monolayer As-graphane is constituted by using As adsorbing on graphane with honeycomb H vacancies. Owing to the surface strain, monolayer As-graphane nanoribbons will self-bend toward the graphane side. The naturally curved As-graphane nanoribbons then exhibit unique spin transport properties, distinctively different from the flat ones, which is a two-dimensional topological insulator. Under external stress, one can realize tunable spin transport in curved As-graphane nanoribon arrays. Such intriguing mechanical bending induced spin flips can offer promising applications in the future nanospintronics devices.

KEYWORDS: Topological insulator, tunable spin transport, graphane, first-principles calculations

Spintronics, using the spin degrees of freedom of the charge carriers, have already been widely studied for potential applications in the spin transistors, spin diodes, memories, and so forth.[1,2] Tuning spin transport properties is a key step in the spintronic devices but remains quite challenging.[3,4] Recently, it has been found that two-dimensional topological insulators (2DTI) exhibit quantum spin Hall (QSH) effect with spin-filtered edge states in the bulk gap.[5−7] More importantly, this topological phase requires neither strong electron−electron interaction nor strong magnetic field to manipulate spin transport, demonstrating a potential paradigm shift in the spintronic devices. Because of the spin-momentum locking property, flat 2DTI nanoribbons present antiparallel spin current along their edges,[7] so that there is no net spin current in a two-terminal settings. However, spin polarizations exist in the curved 2DTI nanoribbons.[8,9] This provides a new path to realizing the spin transport in the curved 2DTI nanoribbons by mechanical bending.[10]

Graphene, a model QSH insulator,[7] is flexible and easy to be bent but has too small spin orbital coupling (SOC) gap. Some theoretical works have indicated that the SOC gap of graphene can be enlarged via metal adatom deposition.[11,12] However, due to the weak interaction between metal adatom and graphene, metal adatoms tend to form nano clusters on graphene.[13−16] Thus, it is quite difficult to obtain monolayer single metal atom-modified metal−graphene systems. Recently, more and more freestanding 2DTIs with large SOC gaps have been predicted,[17−19] and some of them have been synthesized on the substrates.[20−22] Particularly, the large-gap topological insulators have been reported on semiconductor surface, for example, Bi−Si(111),[23] Bi or Pb−Au/Si(111),[24] Bi−Ge(111),[25] and Bi-SiC(111).[26,27] However, owing to the

large thickness of the substrates, none of these systems could be bent easily. Therefore, it is of great interest to look for new flexible 2DTIs to realize the spin polarized transport.[28,29]

In this work, we construct a new QSH insulator named as monolayer As-graphane with As deposition on graphane with honeycomb H vacancies (hHv-graphane), which have been synthesized on the Cu(111) surface.[30] The As-graphane nanoribbons, which curve naturally as a result of the surface stress, will have spin polarized transport properties. Tight-binding (TB) transport calculations also show that the spin polarization depends on the degree of bending of As-graphane nanoribbon. Furthermore, by providing different stress, we are able to tune the spin transport in the curved As-graphane nanoribbon arrays.

Graphane, as a 2D large gap semiconductor, can be synthesized by hydrogenating graphene.[31] Recently, hHv-graphane that contains honeycomb H vacancies have been synthesized on Cu(111) surface.[30] Because of its honeycomb dangling bonds, hHv-graphane is a perfect substrate to grow monolayer honeycomb metal atoms. In Figure 1a, we provide
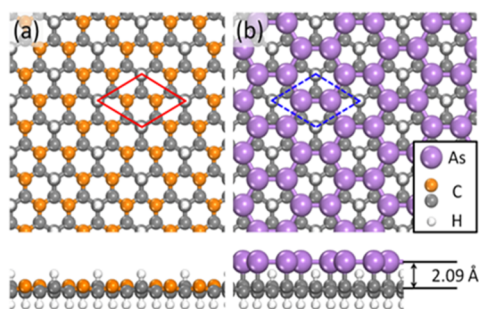

Figure 1. Schematic atomic structure of hHv-graphane and As-graphane film. Top and side view of geometric structure of (a) hHv-graphane and (b) As-graphane. The atoms in gold correspond to the carbon atoms with dangling bonds. The red and blue dash lines denote the unit cells for hHv-graphane and As-graphane, respectively.

the top and side view of the schematic atomic structures for the hHv-graphane, where the atoms in gold correspond to the carbon atoms with dangling bonds. The lattice constant of hHv-graphane is ∼4.37 Å, which is similar to that of the freestanding halogenated arsenene (∼4.6 Å).[32] Hence, we choose As as the adsorbates. All As atoms will bind with the carbon atoms with dangling bonds on the hHv-graphane surface, and form the honeycomb As monolayer. The bonding between As and the underlying C removes effectively the p_z orbital of As, leaving behind a four-band model in a hexagonal lattice, which is known to be topological nontrivial, similar to metal atoms bind on hydrogenated or halogenated Si surface.[23] In Figure 1b, one can see the geometric configurations of the As-graphane system (with new lattice constant of ∼4.465 Å). The distance between As and its nearest carbon atoms is about 2.09 Å, exhibiting strong interactions between them. The binding energy is ∼5.63 eV, which is much larger than that of the cohesive energy of As (∼2.96 eV).[33] The Young's modulus of As-graphane (130.9 GPa) is much smaller than that of graphene (1057.7 GPa) (see Table S1 in the Supporting Information), which suggests that As-graphane is more flexible than graphene. To investigate the dynamic and thermal stability of As-graphane, we calculated its phonon-dispersion curves and found no imaginary frequencies (see Figure S1a in the Supporting Information). We also performed ab initio MD simulations using a supercell of 3 × 3

unit cells at 300 K up to 4 ps and confirmed that the structure of As-graphane is stable (see Figure S1b in the Supporting Information).

Figure 2a shows the band structures and projected density of states (PDOS) of the As-graphane system without and with
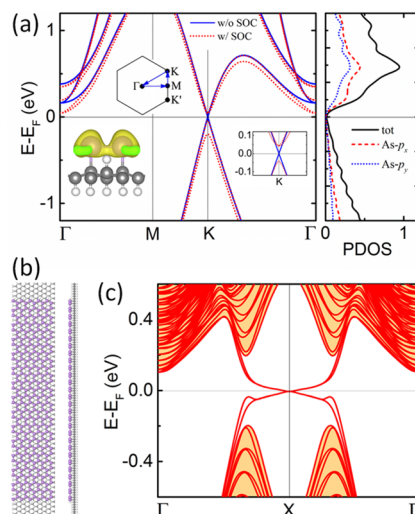

Figure 2. Electronic properties of As-graphane film. (a) Band structures and PDOS, where the left inset indicates the charge distributions around the Fermi level (−0.1−0.1 eV, isosurface = 0.0004 e/Å^3), and the right inset indicates the zoom-in bands around the Fermi level. (b) Top and side view of the flat zigzag As-graphane nanoribbon with a width of ∼10.57 nm (56 As atoms per unit cell). (c) Band structures along the zigzag edge of As-graphane nanoribbon in (b), which clearly exhibit the Dirac edge states of zigzag As-graphane nanoribbon.

SOC. One can see typical Dirac bands exist around the Fermi level. Considering SOC, a band gap (∼83 meV) opens at the Dirac point. From the PDOS, we can confirm that the bands around the Fermi level mainly come from As p_x and p_y orbitals, as also indicated by the plot of partial charge density distribution around the Fermi level. We employ a flat As-graphane zigzag nanoribbon of ∼10.57 nm in width with 56 As atoms per unit cell, as shown in Figure 2b. Figure 2c shows its band structures, where the two linear-dispersion edge states appear. The edge states, connecting the valence and conduction bulk bands and forming a 1D Dirac state at the Brillouin zone boundary, are characterized by an odd number of crossings over the Fermi level (one time at X point), indicating that As-graphane is 2DTI. We also calculate the Z_2 invariant of As-graphane system by using the WCCs methods, and found $Z_2 = 1$ (shown in Figure S2 in the Supporting Information),[34,35] confirming that As-graphane is 2DTI.

Because of a large tensile surface stress in the As-graphane system (about 0.32 eV/Å^2), the zigzag As-graphane nanorib-bons will bend toward the graphane side naturally with a bending curvature 0.41 nm^{-1}.[36] In the left panel of Figure 3a, we show the side view of the geometric structures of the flat zigzag As-graphane nanoribbons containing 16 As atoms per unit cell (with a width of ∼2.84 nm). After full relaxation, the As-graphane nanoribbon bends to the graphane side with a curved angle (the central angle of the curved nanoribbon) ∼ 72°. If we choose an As-graphane nanoribbon containing 40 As atoms per unit cell (with a width of ∼7.48 nm), the curved angle will be up to ∼180°. In Figure 3b, we show the band
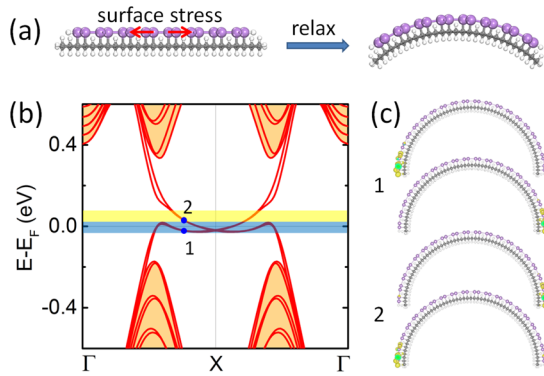
Figure 3. Geometric and electronic structures of naturally curved zigzag As-graphane nanoribbons. (a) Side view of schematic configurations for the curving process of zigzag As-graphane nanoribbon. (b) Band structures of the naturally curved zigzag As-graphane nanoribbon with bending of ~180°. (c) Real-space charge distributions of the edge states at chosen k-points (as marked in b).

Figure 4. Transport properties of the naturally curved As-graphane nanoribbons. TB band structures (a), charge conductance G_c (b), and spin conductance G_s (c) of the naturally curved As-graphane nanoribbon ($\theta \sim 180°$).

structures of the naturally curved As-graphane nanoribbon with bending of ~180°. Similar to the flat As-graphane nanoribbon, there are also gapless edge states inside the bulk band gap. The real-space charge distributions of the edge states at the chosen k-point (as marked in Figure 3b) are shown in Figure 3c. One finds that the charges mainly locate at both edges for the degenerate states, which is the same as that of the flat 2DTI nanoribbons.[37] However, the intriguing difference between their edge states is that the curved case can transport net spin current. For the flat As-graphane nanoribbon, there is only one crossing point between the edge state and Fermi level within the energy window of bulk band gap. For the curved As-graphane nanoribbon, due to the effective second-neighbor hopping, the lower branch of Dirac bands will bend up,[8] and the edge state will be separated into two parts (shaded by yellow and blue in Figure 3b). In the upper part (yellow), there is only one crossing point, which is the same as that in the flat As-graphane nanoribbon. In the lower part (blue), there are three crossing points between the edge state and Fermi level. Therefore, in the lower region the electron backscattering can no longer be 100% prohibited in a scattering process between two states with same energy but different momentum.[37] Neither the three crossing points nor the one crossing point in band gap will change the topological properties, as they are odd numbers. The quantized conductance will be different, where two quantized conductance corresponds to one crossing point and six quantized conductance corresponds to three crossing points, which will be shown in the TB transport calculation results in the following.

To calculate the transport properties of the curved As-graphane nanoribbons, we adopt a spin polarized non-equilibrium Green's function method combined with an As p_x and p_y orbitals based TB Hamiltonian, and the two-center Slater-Koster approximation for hopping.[38] The Hamiltonian takes the form $H = H_{so} + H_0 = \Sigma_i c_i^\dagger H_{ii} c_i + \Sigma_{\langle i,j \rangle \, \mathrm{nbb}} c_i^\dagger H_{ij} c_j$ (where the Rashba terms are neglected).[7] By fitting to the DFT results of the single unit cell As-graphane, we get the TB parameters for the transport calculations (details are shown in the Methods parts). In Figure 4a, we show the TB band structures around the Fermi level for the zigzag As-graphane nanoribbon with bending of ~180°, which are in good agreement with the DFT results in Figure 3b. From Figure 4b, one can clearly see that the charge conductance is quantized ($2e^2/h$), and the two peaks
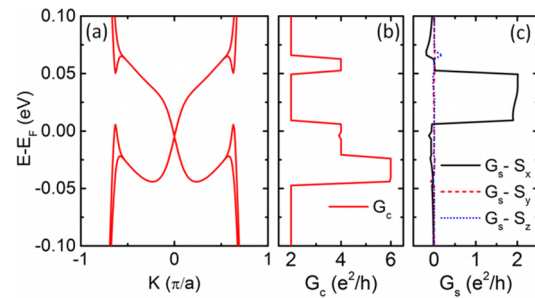
in the charge conductance around the Fermi level come from the band splitting at the edge of the SOC gap. The spin conductance along different directions are shown in Figure 4c. Only spin conductance along x direction is not zero. The spin conductance mainly comes from two edge states propagating in the same direction. If we define S_x, S_y, S_z as the x-, y-, and z-directional components of the spin current S, these two edge states contribute zero S_z spin current, the same S_x spin current, and the opposite S_y spin current. Thus, only the x-component contributes to the spin conductance. This spin conductance spectrum is intrinsic for the considered structure, and can be obtained without magnetization field. More importantly, the polarization happens only in the Dirac energy bands near the Fermi energy (in the SOC gaps of 2DTI).

According to our previous calculation, only the x-component contributes to the spin conductance. Then, we can use the formula $G_s = G_c \cos\left(\frac{\pi - \theta}{2}\right) = 2 \cos\left(\frac{\pi - \theta}{2}\right)$ to estimate the spin conductance for different curved angles θ. From this formula, we can find that the spin conductance will increase as the bending increases. Then, we can realize the tuned spin conductance through tuning the bending of As-graphane nanoribbons. Here, we construct a new periodic model, named as zigzag As-graphane nanoribbon array.[39] In this model, there are 40 As atoms (with a width of ~7.48 nm) located on graphane nanoribbon which contains 204 C atoms (with a width of ~12.7 nm) per unit cell. After relaxation, the flat zigzag As-graphane nanoribbon arrays will shrink along the ribbon width direction and form the curved ones (shown in Figure S5 in the Supporting Information). Because the extra graphene nanoribbon provides tensile surface stress along the opposite direction, the curved angle θ of the relaxed structure is ~168°, which is a slightly smaller than that in the naturally curved As-graphane nanoribbon. We can use different external stress to get As-graphane arrays with different curved angles. Compressive strain (tensile strain) will increase (decrease) the curved angle θ. In Figure 5a, we show the geometric structures of the strain tuned As-graphane arrays with four different curved angles θ, 0, $\pi/3$, $2\pi/3$, and π, corresponding to four strains, 65.4%, 56.6%, 34.0%, and −1.9%, respectively. Figure 5b shows their corresponding spin conductances, respectively. Clearly, the spin conductance obeys the formula $G_s = 2 \cos\left(\frac{\pi - \theta}{2}\right)$, where $G_{s\text{-}2\pi/3} \approx 1.7$, $G_{s\text{-}\pi/3} \approx 1$, and $G_{s\text{-}0} = 0$. Thus, we demonstrate the tuned spin conductance in the zigzag As-graphane nanoribbon arrays by strain.

In summary, we construct a new QSH insulator named as monolayer As-graphane and find that the naturally curved As-
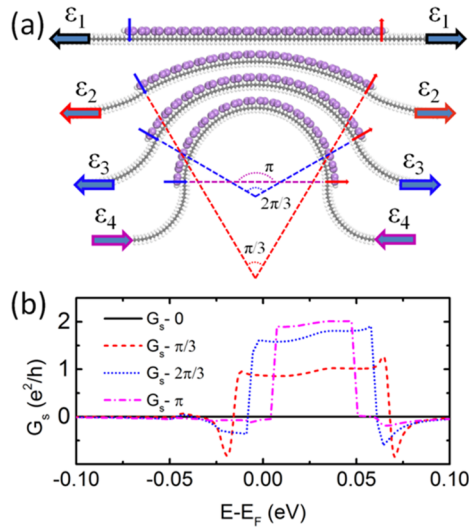
Figure 5. Spin transport for the strain tuned zigzag As-graphane nanoribbon arrays. (a) Geometric structures of the strain tuned zigzag As-graphane nanoribbon arrays with different curved angles, and (b) their corresponding spin conductivities G_s.

graphane nanoribbons exhibit spin polarized transport properties. The spin transport properties are intrinsic, and the spin polarizations can be obtained without external magnetization field. By applying different external strain, we can realize 0−100% spin polarizations. The strain tuned spin transport properties in the As-graphane nanoribbon arrays provide a perfect tunable spin injector (schematic design is shown in Figure S6 in the Supporting Information), which may offer promising applications in spintronic devices.

■ METHODS

DFT Computations. All DFT calculations are carried out using Vienna ab initio simulation package (VASP)[40] with the projector augmented wave method, and a generalized gradient approximation (GGA) in the form of Perdew−Burke−Ernzerhof (PBE) is adopted for the exchange-correlation functional.[41] The energy cutoff of the plane-wave basis set is 400 eV. When doing the static self-consistent calculations, $15 \times 15 \times 1$ and $1 \times 1 \times 5$ Monkhorst-Park k-point meshes are used for the single unit cell of As-graphane and As-graphane nanoribbons, respectively. In all the calculations, a 15 Å vacuum layer is used and all atoms are fully relaxed until the residual forces on each atom are smaller than 0.01 eV/Å. The Z_2 invariant is determined by the evolution of the Wannier Charge Centers (WCCs) method.[34,35]

Tight Binding Models and Transport Computations. For all the As-graphane systems (consisting of freestanding single unit cell As-graphane, as well as flat and curved As-graphane nanoribbons), we adopt a spinful tight-binding model with As p_x and p_y orbitals and the two-center Slater-Koster approximation[38] for hopping. For cases that the SOC gap is larger than the Rashba splitting, to simplify our calculation, we neglect the Rashba term. The tight-binding Hamiltonian takes the form

$$H = H_{so} + H_0 = \sum_i c_i^+ H_{ii} c_i + \sum_{\langle i,j \rangle} c_i^+ H_{ij} c_j \tag{1}$$

where $c_i^+ = (c_{ix\uparrow}^+, c_{ix\downarrow}^+, c_{iy\uparrow}^+, c_{iy\downarrow}^+)$ contains the creation operators of the electron on the orbital $p_{ix\uparrow}$, $p_{ix\downarrow}$, $p_{iy\uparrow}$, $p_{iy\downarrow}$ at site i, and $\langle i,j \rangle$

indicates that the site i and j are the nearest neighbor. We take the atomic energy of p orbitals as the zero of energy. Then the on-site energy H_{ii} includes only the spin−orbit coupling[8]

$$H_{ii} = \begin{bmatrix} 0 & -i\lambda\boldsymbol{\sigma}\cdot\mathbf{e}_z/2 \\ i\lambda\boldsymbol{\sigma}\cdot\mathbf{e}_z/2 & 0 \end{bmatrix} \tag{2}$$

where λ represents the strength of atomic spin−orbit coupling, and $\boldsymbol{\sigma}$ is the vector of Pauli matrices.

The hopping matrix H_{ij} is given by

$$H_{ij} = \begin{bmatrix} t_{xx}\sigma_0 & t_{xy}\sigma_0 \\ t_{yx}\sigma_0 & t_{yy}\sigma_0 \end{bmatrix} \tag{3}$$

where $t_{\alpha\beta} = A_{\alpha\beta}t_{pp\sigma} + (\mathbf{e}_\alpha\cdot\mathbf{e}_\beta - A_{\alpha\beta})t_{pp\pi}$, σ_0 is the 2×2 unit matrix, $A_{\alpha\beta} = (\mathbf{e}_\alpha\cdot\mathbf{e}_{ij})(\mathbf{e}_\beta\cdot\mathbf{e}_{ij})$ with $\mathbf{e}_{ij}$ as the unit vector directed from site i to j, and $t_{pp\sigma}$ and $t_{pp\pi}$ are hopping parameters.

When the orbitals from different sites (i and j) are nonorthogonal, the overlap integral between them should be considered through an overlap matrix S_{ij}. By means of the overlapping parameters $S_{pp\sigma}$ and $S_{pp\pi}$, one has $\langle p_{i\alpha}|S|p_{j\beta}\rangle = [A_{\alpha\beta}S_{pp\sigma} + (\mathbf{e}_\alpha\cdot\mathbf{e}_\beta - A_{\alpha\beta})S_{pp\pi}]\sigma_0$. Note that S_{ii} is a 4×4 unit matrix.

For the freestanding single unit cell As-graphane, by fitting with the DFT results we get the strength of atomic spin−orbit coupling, the corresponding hopping and overlapping parameters $\lambda = 0.09$, $t_{pp\sigma} = 1.3$, $t_{pp\pi} = -1.0$, $S_{pp\sigma} = -0.05$, $S_{pp\pi} = 0.6$. The fitting results are shown in Figure S4 in the Supporting Information, we can find the TB results agree well with the first principle results.

For the As-graphane nanoribbons, we adopt a global coordinate system XYZ shown in Figure S3 in the Supporting Information to describe the spin vectors. The OZ axis is in parallel with the primitive lattice vector **a** of the ribbon, which is taken as the spin quantum axis. At each site i, a local coordinate system $\mathbf{e}_x$, $\mathbf{e}_y$, and $\mathbf{e}_z$ is used to define the three p-orbitals. Here the unit vector $\mathbf{e}_x$ is along the Z direction, $\mathbf{e}_y = \mathbf{e}_z \times \mathbf{e}_x$, and $\mathbf{e}_z$ is oriented along the line from the bonded carbon atom to the As atom at site i. Note that we neglect the component of $\mathbf{e}_z$ along $\mathbf{e}_x$ because $|\mathbf{e}^z\cdot\mathbf{e}^x| \ll 1$. The lobe of the p-orbital $p_{ix/y/z}$ at site i is pointing along $\mathbf{e}_{x/y/z}$. The strength of atomic SOC, the hopping parameters $t_{pp\sigma}$ and $t_{pp\pi}$ and overlapping parameters $S_{pp\sigma}$ and $S_{pp\pi}$ are the same as the fitting ones on the freestanding single unit cell As-graphane, and the second-neighbor hopping parameters are 10% of that of the nearest hopping parameters.

The Bloch eigenstate with one-dimensional wave vector k can be written as $|\psi\rangle = \Sigma_i c_i^+|0\rangle\psi_i$, where the four-component wave function ψ_i satisfies $\Sigma_j H_{ij}\psi_j = E\Sigma_j S_{ij}\psi_j$. Further, if the position difference between site i and j is na (n is integer), then $\psi_i = \exp(inka)\psi_j$. For the eigenstate $|\psi\rangle$, the local spin density $\langle \vec{s}_i\rangle$ and probability density $\langle \rho_i\rangle$ at site i are obtained from

$$\langle \vec{s}_i\rangle = \tilde{\psi}_i^+(\sigma_0 \otimes \vec{\sigma})\tilde{\psi}_i, \quad \langle \rho_i\rangle = \tilde{\psi}_i^+\tilde{\psi}_i, \quad \tilde{\psi}_i = \sum_j S_{ij}\psi_j \tag{4}$$

For a given k point, there may exist two degenerate states. In this case, we introduce a tiny magnetization field **m** (**m** < 0.2 meV) to break the degeneracy so that each state can be attributed to an intrinsic spin density.[8] This would only change the onsite energy H_{ii} in (2), whose diagonal blocks become **m**·$\boldsymbol{\sigma}$.

To examine the spin current in the curved ribbon, we apply a voltage bias V along the ribbon direction so that the electric

potential is $-V/2$ in the region $z < 0$ and $V/2$ in the region $z > L_z$ (where L_z is the length of the curved ribbon). In the middle region $0 < x < L_z$, the electric potential is assumed to have a linear profile. The Fermi energy at zero bias is set at zero.

At zero temperature, the spin current flowing through the region $z > L_z$ can be calculated from[42]

$$I_s^\alpha = \frac{e}{h} \int_{-eV/2}^{eV/2} T_\alpha(E, V)\,dE, \qquad T_\alpha = \mathrm{Tr}[(1_N \otimes \sigma_\alpha)\Gamma_2 G \Gamma_1 G^+] \tag{5}$$

where I_s^α is the current of the spin α component ($\alpha = x, y, z$) divided by $\hbar/2$, $T_\alpha(E,V)$ is spin-dependent transmission, the broadening function $\Gamma_p = i(\Sigma_p - \Sigma_p^+)$ is expressed in terms of the retarded self-energy Σ_p ($p = 1, 2$ for the region $z < 0$ and $z > L_z$), G is the retarded Green's function, and 1_N is a unit matrix. (If we change σ_α in eq 5 as σ_0, we will get the charge transmission T_0 and the charge current I^0.)

■ ASSOCIATED CONTENT

ⓢ Supporting Information

The Supporting Information is available free of charge on the ACS Publications website at DOI: 10.1021/acs.nano-lett.7b01438.

> Independent elastic constant for As-graphane and graphene, phonon-dispersion curve and snapshots from MD simulation of As-graphane at 300 K after 4fs, Z2 invariant calculations of the As-graphane, schematic atomic structure of the naturally curved zigzag As-graphane nanoribbons, the comparison between first-principles and TB band structures of As-graphane, schematic atomic structure of the naturally curved As-graphane nanoribbon arrays, and schematic design of a proposed strain turned spin injector (PDF)

■ AUTHOR INFORMATION

Corresponding Authors
*E-mail: zhmwang@uestc.edu.cn.
*E-mail: fliu@eng.utah.edu.
ORCID Ⓘ
L. Z. Zhang: 0000-0001-9838-8178
Notes
The authors declare no competing financial interest.

■ ACKNOWLEDGMENTS

■ REFERENCES

(1) Wolf, S. A.; Awschalom, D. D.; Buhrman, R. A.; Daughton, J. M.; Molnár, S. von; Roukes, M. L.; Chtchelkanova, A. Y.; Treger, D. M. Science 2001, 294, 1488−1495.

(2) Zutic, I.; Fabian, J.; Das Sarma, S. Rev. Mod. Phys. 2004, 76, 323−410.

(3) Sahoo, S.; Kontos, T.; Furer, J.; Hoffmann, C.; Gräber, M.; Cottet, A.; Schönenberger, C. Nat. Phys. 2005, 1, 99−102.

(4) Appelbaum, I.; Huang, B.; Monsma, D. J. Nature 2007, 447, 295−298.

(5) Hasan, M. Z.; Kane, C. L. Rev. Mod. Phys. 2010, 82, 3045.

(6) Qi, X.-L.; Zhang, S.-C. Rev. Mod. Phys. 2011, 83, 1057.

(7) Kane, C. L.; Mele, E. J. Phys. Rev. Lett. 2005, 95, 226801.

(8) Gosálbez-Martínez, D.; Palacios, J. J.; Fernández-Rossier, J. Phys. Rev. B: Condens. Matter Mater. Phys. 2011, 83, 115436.

(9) Jin, K. H.; Jhi, S. H. Phys. Chem. Chem. Phys. 2016, 18, 8637−8642.

(10) Huang, B.; Jin, K.; Cui, B.; Zhai, F.; Mei, J. W.; Liu, F. Nat. Commun. 2017, 8, 15850.

(11) Weeks, C.; Hu, J.; Alicea, J.; Franz, M.; Wu, R. Q. Phys. Rev. X 2011, 1, 021001.

(12) Hu, J. A.; Alicea, J.; Wu, R. Q.; Franz, M. Phys. Rev. Lett. 2012, 109, 266801.

(13) Wang, B.; Bocquet, M. − L. J. Phys. Chem. Lett. 2011, 2, 2341.

(14) Zhang, L. Z.; Du, S. X.; Sun, J. T.; Huang, L.; Meng, L.; Xu, W. Y.; Pan, L. D.; Pan, Y.; Wang, Y. L.; Hofer, W. A.; Gao, H. J. Adv. Mater. Interfaces 2014, 1, 1300104.

(15) N'Diaye, A. T.; Bleikamp, S.; Feibelman, P. J.; Michely, T. Phys. Rev. Lett. 2006, 97, 215501.

(16) Zhou, H. Q.; Qiu, C. Y.; Yang, H. C.; Hu, L. J.; Liu, J.; Yang, H. F.; Gu, C. Z.; Sun, L. F. J. Am. Chem. Soc. 2010, 132, 944.

(17) Liu, C.-C.; Feng, W.; Yao, Y. G. Phys. Rev. Lett. 2011, 107, 076802.

(18) Liu, Z.; Liu, C.-X.; Wu, Y.-S.; Duan, W.-H.; Liu, F.; Wu, J. Phys. Rev. Lett. 2011, 107, 136805.

(19) Xu, Y.; Yan, B.; Zhang, H.-J.; Wang, J.; Xu, G.; Tang, P.; Duan, W.; Zhang, S.-C. Phys. Rev. Lett. 2013, 111, 136804.

(20) Vogt, P.; De Padova, P.; Quaresima, C.; Avila, J.; Frantzeskakis, E.; Asensio, M.; Resta, A.; Ealet, B.; Le Lay, G. Phys. Rev. Lett. 2012, 108, 155501.

(21) Yang, F.; Miao, L.; Wang, Z. F.; Yao, M.-Y.; Zhu, F.; Song, Y. R.; Wang, M.-X.; Xu, J.-P.; Fedorov, A. V.; Sun, Z.; Zhang, G. B.; Liu, C.; Liu, F.; Qian, D.; Gao, C. L.; Jia, J.-F. Phys. Rev. Lett. 2012, 109, 16801.

(22) Zhu, F. F.; Chen, W. J.; Xu, Y.; Gao, C. L.; Guan, D. D.; Liu, C. L.; Qian, D.; Zhang, S. C.; Jia, J. F. Nat. Mater. 2015, 14, 1020−1025.

(23) Zhou, M.; Ming, W.; Liu, Z.; Wang, Z.; Li, P.; Liu, F. Proc. Natl. Acad. Sci. U. S. A. 2014, 111, 14378−14381.

(24) Huang, B.; Jin, K. − H.; Zhuang, H. L.; Zhang, L. Z.; Liu, F. Phys. Rev. B: Condens. Matter Mater. Phys. 2016, 93, 115117.

(25) Li, P.; Zhou, M.; Zhang, L.; Guo, Y.; Liu, F. Nanotechnology 2016, 27, 095703.

(26) Hsu, C.; Huang, Z.; Chuang, F.; Kuo, C.; Liu, Y.; Lin, H.; Bansil, A. New J. Phys. 2015, 17, 025005.

(27) Reis, F.; Li, G.; Dudy, L.; Bauernfeind, M.; Glass, S.; Hanke, W.; Thomale, R.; Schäfer, J.; Claessen, R. 2016, arXiv: 1608.00812.

(28) Liu, C. C.; Guan, S.; Song, Z. G.; Yang, S. A.; Yang, J. B.; Yao, Y. G. Phys. Rev. B: Condens. Matter Mater. Phys. 2014, 90, 085431.

(29) Luo, W.; Xiang, H. J. Nano Lett. 2015, 15, 3230−3235.

(30) Lin, C.; Feng, Y.; Xiao, Y.; Dürr, M.; Huang, X.; Xu, X.; Zhao, R.; Wang, E.; Li, X.; Hu, Z. Nano Lett. 2015, 15, 903−908.

(31) Elias, D. C.; Nair, R. R.; Mohiuddin, T. M. G.; Morozov, S. V.; Blake, P.; Halsall, M. P.; Ferrari, A. C.; Boukhvalov, D. W.; Katsnelson, M. I.; Geim, A. K.; Novoselov, K. S. Science 2009, 323, 610−623.

(32) Wang, D. C.; Chen, L.; Shi, C. M.; Wang, X. L.; Cui, G. L.; Zhang, P. H.; Chen, Y. Q. Sci. Rep. 2016, 6, 28287.

(33) Kittel, C. Introduction to Solid State Physics, 8th ed.; Wiley: New York, 2005.

(34) Soluyanov, A. A.; Vanderbilt, D. Phys. Rev. B: Condens. Matter Mater. Phys. 2011, 83, 235401.

(35) Soluyanov, A. A.; Vanderbilt, D. Phys. Rev. B: Condens. Matter Mater. Phys. 2011, 83, 035108.

(36) Yu, D. C.; Liu, F. Nano Lett. 2007, 7, 3046−3050.

(37) Wang, Z. F.; Chen, L.; Liu, F. Nano Lett. 2014, 14, 2879−2883.

(38) Slater, J. C.; Koster, G. F. Phys. Rev. 1954, 94, 1498.

(39) Wang, Z. F.; Zhang, Y.; Liu, F. Phys. Rev. B: Condens. Matter Mater. Phys. 2011, 83, 041403.

(40) Kresse, G.; Furthmuller, J. *Phys. Rev. B: Condens. Matter Mater. Phys.* **1996**, *54*, 11169.

(41) Perdew, J. P.; Burke, K.; Ernzerhof, M. *Phys. Rev. Lett.* **1996**, *77*, 3865.

(42) Chang, P. H.; Mahfouzi, F.; Nagaosa, N.; Nikolic, B. K. *Phys. Rev. B: Condens. Matter Mater. Phys.* **2014**, *89*, 195418.